Journal of Medicinal Chemistry

Article

pubs.acs.org/jmc

Identification of a Novel Aminotetralin Class of HDAC6 and HDAC8 Selective Inhibitors

Guozhi Tang,* Jason C. Wong,† Weixing Zhang, Zhanguo Wang, Nan Zhang, Zhenghong Peng, Zhenshan Zhang, Yiping Rong, Shijie Li, Meifang Zhang, Lingjie Yu, Teng Feng, Xiongwen Zhang, Xihan Wu, Jim Z. Wu, and Li Chen

Roche Pharmaceutical Research and Early Development, Roche Innovation Center Shanghai, 720 Cailun Road, Shanghai, 201203 China

Supporting Information

ABSTRACT: Herein we report the identification of a novel class of HDAC6 and HDAC8 selective inhibitors through a unique chemistry and phenotypic screening strategy. Tetrahydroisoquinoline **12** was identified as a potent HDAC6 and HDAC8 dual inhibitor from a focused library through cellular tubulin acetylation and p21 induction screening assays. Scaffold hopping from **12** led to the discovery of an aminotetralin class of HDAC inhibitors. In particular, the 3-*R* stereoisomer **32** showed highly potent inhibition against HDAC6 and HDAC8 with IC_{50} values of 50 and 80 nM, respectively. Treatment of neuroblastoma BE(2)C cells with **32** resulted in elevated levels of acetylated tubulin, TrkA, and neurite outgrowth with only marginal effects on p21 induction and histone H3 acetylation. Consistent with its weak enzymatic inhibition of HDAC1, **32** showed significantly less cytotoxicity than SAHA and moderately inhibited the growth of myeloma NCI-H929 and OPM-2 cells.

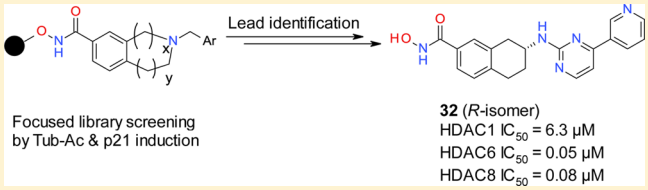

INTRODUCTION

Histone deacetylases (HDACs) are one of the major classes of post-translational regulators that are responsible for deacetylation of lysine residues in histone and non-histone substrates.[1] There are 18 HDAC isoforms that are divided into four classes based on their sequence similarity, cellular localization, tissue expression patterns, and enzymatic mechanisms. Class I (HDACs 1, 2, 3, and 8), class II (HDACs 4, 5, 6, 7, 9, and 10), and class IV (HDAC11) HDACs are all zinc-dependent deacetylases that are mechanistically distinct from NAD^+-dependent class III HDACs. Inhibition of HDACs is a proven epigenetic strategy for the treatment of cancers, evidenced by the fact that both vorinostat (SAHA) and romidepsin (FK-228) have gained FDA approval for the treatment of cutaneous T-cell lymphoma (CTCL). In addition, there are additional HDAC inhibitors at various stages of clinical development for the treatment of hematological malignancies, solid tumors, and immunological or neurological disorders. Most of them are class I selective, such as romidepsin, chidamide (CS-055), entinostat (SNDX-275), or pan-HDAC inhibitors such as SAHA and LBH-589. Selective HDAC inhibitors that affect only a limited number of isoforms are valuable, as they can be used as tools to study the roles of individual HDAC isoforms in biological processes and as potential therapeutic agents to treat certain diseases with potentially fewer side effects than pan-HDAC inhibitors.[2]

The HDAC inhibitors typically share a well-recognized pharmacophore that consists of three parts: (1) a zinc-binding group (ZBG) that is buried deep in the catalytic pocket of the HDAC enzyme to chelate with the zinc cation and form key hydrogen bonding interactions with the surrounding active site residues; (2) a linker that passes through the narrow hydrophobic channel of HDACs; and (3) a partially exposed capping group that interacts with the rim region where HDAC isoforms have significant structural variation and conformational plasticity. Practically, the structural difference of HDACs has been exploited successfully and isoform selectivity can be generated from modulation of ZBG and appropriate conformational constraints in the linker or capping groups. Tubacin (**1**),[3] ACY-1215 (**2**),[4] tubastatin (**3**),[5] and HPOB (**4**)[6] are reported as HDAC6 selective inhibitors using bulky or conformationally constrained capping groups as selectivity vector (Figure 1). Conformational constraint at the linker part is also widely applied to generate HDAC isoform selectivity, as exemplified by HDAC6 inhibitor BRD9757 (**5**)[7] and HDAC8 inhibitors PCI-34051 (**6**)[8] and NCC149 (**7**).[9] In particular, **5** is capping-free and it uses a cyclopentene moiety for HDAC6 selectivity. For the ZBG part of HDAC inhibitors, it is generally limited to hydroxamic acid, thiol, carboxylic acid, and ketone groups. But there are a few successful cases where atypical ZBGs were devised for generation of HDAC isoform selectivity. Different from other HDAC isoforms, HDAC1−3 are reported to possess a larger exit channel at the catalytic site that tolerates bulky ZBGs like *o*-aminoanilide. Both SNDX-275 and chidamide belong to this class of HDAC inhibitors that target HDAC1−3 only.[10,11]

Received: June 12, 2014
Published: September 19, 2014

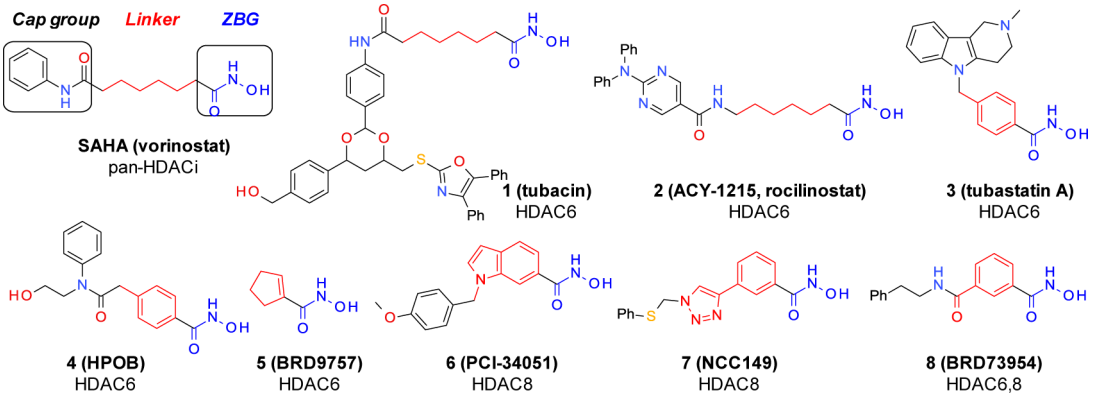

Figure 1. SAHA and known HDAC6/HDAC8-selective inhibitors.

Scheme 1. Solid Phase Synthesis of Focused Libraries and Identification of 12 as HDAC6/8 Inhibitor

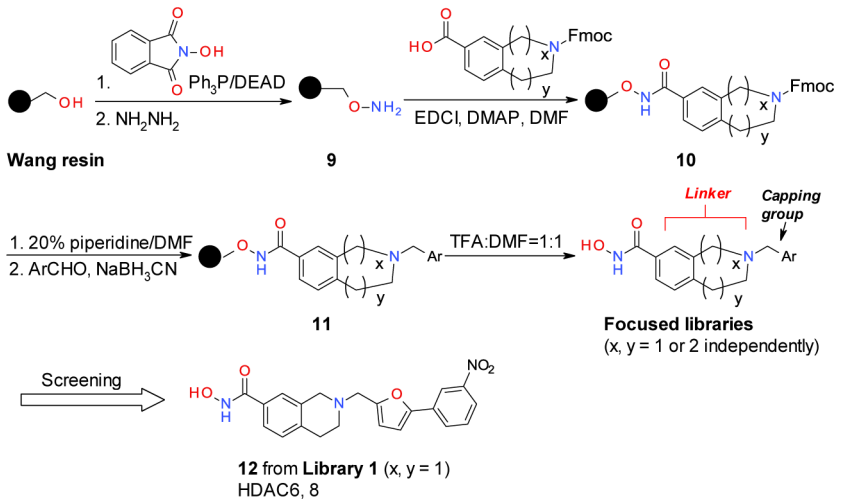

Previously, we disclosed 3*R*,4*S*-pyrrolidines as HDAC1−3 selective inhibitors that demonstrated dose dependent in vivo antitumor efficacy in xenograft models with concurrent induction of p21 and acetylated histone H3 in tumor tissues.[12] Herein we report our efforts to discover and characterize novel HDAC inhibitors with specific HDAC isoform selectivity, especially toward HDAC6 and/or HDAC8. Selective inhibition of HDAC6 has recently emerged as an attractive approach for the treatment of cancers, Alzheimer's disease, and rheumatoid arthritis.[13] For example, **2** currently is in phase I/II clinical trials for treatment of multiple myeloma.[4] While originally disclosed as a neuroprotective agent, **3** and its *β*- and *γ*-carboline analogues were found to enhance the immunosuppressive effects of Foxp3+ regulatory T cells and have anti-inflammatory effects.[5] Notably, **4** did not induce cell death by itself but enhanced the effectiveness of DNA-damaging anticancer drugs in transformed cells but not normal cells.[6] On the other hand, HDAC8 has been implicated as a drug target for the treatment of minimal residual disease in neuroblastoma and malignancies such as T-cell lymphoma and acute myeloid leukemia.[14] HDAC8 inhibitors such as **6** and **7** were reported to induce apoptosis and exert growth-inhibitory effects on T-cell lymphoma cells.[8,9] Recently, E. Holson et al. reported the identification of a meta-substituted phenylhydroxamic acid **8** as an HDAC6/8 dual inhibitor based on enzymatic inhibition profile against selected HDAC isoforms.[15] It has been suggested that simultaneous inhibition of HDAC6 and HDAC8 has many potential therapeutic applications, providing a larger therapeutic window than inhibition of HDAC1−3.[13−15]

RESULTS AND DISCUSSION

We considered conformational constriction of the linker as the most effective approach to devise HDAC isoform-selectivity with high ligand efficiency. Since hydroxamic acids are usually complicated by hydrolysis issues and suboptimal solubility, a focused library was designed and prepared by facile solid phase synthesis using reductive amination to connect fused bicyclic linkers and various capping groups (Scheme 1). In library synthesis, "Wang" resin was loaded with *N*-hydroxyphthalimide by Mitsunobu reaction and then treated with hydrazine to generate resin **9**. A coupling reaction of **9** and benzoic acids that have six- or seven-member fused rings gave **10** (see details in Supporting Information). After removal of the *N*-Fmoc protective groups by piperidine, the secondary amine was coupled with different aromatic aldehydes and the resulting Schiff base was reduced with $NaBH_3CN$ to afford **11**. Ultimately, hydroxamates were released from resin **11** upon treatment with TFA and purified by preparative HPLC. The synthesized compounds were then evaluated in tubulin acetylation assay (Tub-Ac)[16] as a surrogate for cellular HDAC6 inhibition. As a surrogate assay for HDAC1−3 inhibition, p21 reporter gene assay[17] was applied as a counterscreen using SNDX-275 as the standard reference for selectivity assessment.

dx.doi.org/10.1021/jm5008962 | J. Med. Chem. 2014, 57, 8026−8034

Among those moieties used as linkers, the 2,7-disubstituted tetrahydroisoquinoline class was found to possess the desired selectivity profile. For example, analogue **12** showed strong Tub-Ac activities and low p21 induction in cellular assays. In the cellular HDAC6 inhibition assay, **12** showed about 70% of Tub-Ac when compared to SAHA at 10 and 30 μM, respectively, with EC_{50} at 3.45 μM. In the counterscreen against HDAC1−3 isoforms, **12** did not induce p21 when compared to SNDX-275 at 3, 10, and 30 μM in HeLa cells (Table 1). **12** was then biochemically profiled against a panel of

Table 1. Tubulin Acetylation and p21 Reporter Gene Induction by 17−28[a]

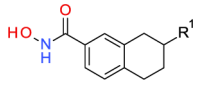

ID	R^1 (Cap group)	EC_{50} (Tub-Ac, μM) [a]	p21-RP3 [b]	p21-RP10 [b]	LYSA [c]
SAHA		1.03	4030%	850%	311
12	-	3.45	11%	0%	6
17		12.45	-7%	-1%	190
18		0.46	-2%	-8%	< 1
19		5.0	-9%	-1%	226
20		0.73	-	-1%	37
21	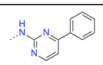	1.31	-58%	-8%	12
22	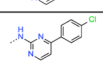	8.70	-22%	-20%	< 1
23	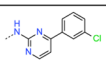	4.95	-68%	-59%	< 1
24	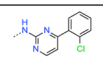	0.93	30%	0%	8
25	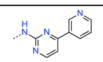	1.18	-33%	-2%	66
26	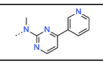	2.25	-38%	-10%	12
27	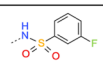	0.99	18%	26%	109
28	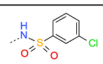	1.72	52%	31%	85

[a] EC_{50} values of tubulin acetylation are based on ELISA experiments run in duplicate in A549 cells, SD ± 15%. [b] p21-RP3 represents the relative luciferase signal in the p21 reporter gene assay[17] by individual example compared to SNDX-275[10] at 3 μM in triplicate and normalized by internal GFP transfection control; p21-RP10 represents the relative level of p21 induced by individual example compared to SNDX-275 at 10 μM in triplicate. In all cases data varied by 10% or less. [c] The lyophilized solubility assay (LYSA) was run in duplicate. The mean values are reported in μg/mL, SD ± 10%.

all 11 zinc-dependent HDACs. It inhibited enzymatic activities of HDAC6 and HDAC8 with IC_{50} values of 0.05 and 0.03 μM, respectively, but was barely active against other HDAC isoforms with an IC_{50} of 6.6 μM against HDAC3 and above 20 μM against other HDACs (Table 2). These results indicated that **12** is a selective HDAC6/8 inhibitor and a good starting point for further chemistry optimization. We then evaluated the in vitro metabolic stability and physiochemical properties of compound **12**. It had high intrinsic clearance largely due to hydrolysis of the hydroxamic acid group and N−C cleavage on the tetrahydroisoquinoline moiety based on microsome metabolite identification studies. Compound **12** also had poor solubility at less than 10 μg/mL in the lyophilized solubility assay (LYSA). To address these metabolic stability and solubility issues, an aminotetralin class of analogues **17**−**25** were designed in close mimicry to the linker of **12** and synthesized according to the procedures in Scheme 2. Ketone derivative **13** was converted to *N*-Boc aminotetralin **14** by an amination reaction and then treatment with $(Boc)_2O$. After the Pd-catalyzed carboxylation and removal of Boc protective group, **15** was obtained. It was treated with different aryl halides under copper-catalyzed coupling or nucleophilic aromatic substitution conditions to incorporate the capping groups. The resultant ester **16** was treated with hydroxylamine under basic conditions to give hydroxamic acids **17**−**25**. In addition, a few N-methylated analogues such as **26** and sulfonamides **27** and **28** were made to explore the structure−activity relationship (SAR) and HDAC isoform selectivity.

These aminotetralin-based hydroxamates were evaluated for their biological effects on Tub-Ac and p21 induction in cellular assays. We anticipated that various capping groups would form important hydrophobic interactions with the water-exposed residues at the rim region and that heteroaromatic groups and polar functional groups would be tolerated or even beneficial at this position. Accordingly, the 2-aminopyrimidine analogue **20** showed significantly enhanced cellular HDAC6 inhibition over aniline analogue **17** and the 2-aminopyridine analogue **19**. It remains unclear if this was due to extra hydrogen bonding or increased $\pi-\pi$ interactions between the electron-deficient pyrimidine group and certain HDAC6 residues. It was found that a phenyl group was well tolerated at the meta-position of the aminopyrimidine ring but any further substitution on the phenyl group did not necessarily contribute to potency or selectivity (see examples **21**−**24**). Finally, we found that analogue **25** with a pyridine substituent at the meta-position demonstrated potent Tub-Ac induction with an EC_{50} of 1.18 μM and had good solubility with LYSA of 66 μg/mL. N-methylation typically led to decreased Tub-Ac induction as indicated by analogue **26**. While sulfonamide analogues had good potency in Tub-Ac, it came with a loss of selectivity against HDAC1−3. For example, sulfonamides **27** and **28** had consistent p21 induction at 3 and 10 μM, respectively. We speculate that the sulfonamide capping groups have a different orientation relative to the linker and are thus better tolerated by HDAC1−3 isoforms than non-sulfonamides **17**−**26**.

We decided to further study racemate **25** to clarify the impact of its stereochemistry on HDAC6/8 inhibition. Optically pure *tert*-butyl *N*-(7-bromotetralin-2-yl)carbamates **29** and **30** were obtained by supercritical fluid chromatography (SFC) chiral separation of **14**, and the stereochemistry of **30** (2*R*) was confirmed by X-ray structure (Supporting Information). By following the same procedure used to prepare **25**, chiral hydroxamates **31** (*S*) and **32** (*R*) were synthesized from **29** and **30** independently (Scheme 3).

In agreement with the results of **25**, neither **31** nor **32** induced p21 in HeLa cells at 3 and 10 μM relative to SNDX-275 (Figure 2A). In contrast, SAHA, a nonselective HDAC inhibitor, demonstrated 8−40 times more p21 induction than SNDX-275 under the same concentrations. Meanwhile, both **31** and **32** potently induced tubulin acetylation with EC_{50} values of 0.69 and 1.64 μM, respectively, which are similar to the activity of SAHA (Figure 2B). The cellular assays indicated

dx.doi.org/10.1021/jm5008962 | J. Med. Chem. 2014, 57, 8026−8034

Table 2. Biological Activities of 31 and 32

	IC_{50} against HDAC isoforms (μM)[a,c]											GI_{50} (μM)[b,c]	
compd	HDAC1	HDAC2	HDAC3	HDAC4	HDAC5	HDAC6	HDAC7	HDAC8	HDAC9	HDAC10	HDAC11	NCI-H929	BE(2)-C
SAHA	0.31	0.24	0.13	76.0	27.2	0.20	105	0.31	141	0.43	0.20	0.8	1.1
12	21.3	109.0	6.59	67.8	36.0	0.05	60.7	0.03	65.8	71.1	75.3	–	5.1
31	11.2	–	–	–	–	0.04	–	0.39	–	–	–	–	16.1
32	6.31	>100	>100	>100	>100	0.05	30.8	0.08	35.0	>100	>100	7.7	5.4

[a]IC_{50} values of enzymatic inhibition to HDAC enzymes run in duplicate, SD ± 15%. IC_{50} values of SAHA are cited from www.reactionbiology.com. Inhibition assays were performed by Reaction Biology Corporation according to their standard assay protocols; see Supporting Information. [b]Growth inhibition in cancer cell lines. Values are the mean of three determinations run in duplicate, SD ± 20%. [c]"–" represents not determined.

Scheme 2. Synthesis of Aminotetralin Linked Analogues 17–28[a]

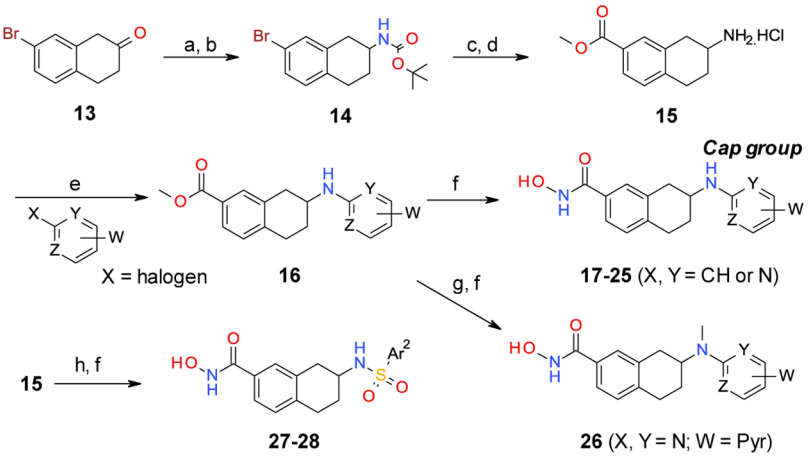

[a]Reagents and conditions: (a) NH_4OAc, $NaBH_3CN$, rt, overnight; (b) $(Boc)_2O$, NEt_3, rt, 2 h; (c) $Pd(OAc)_2$, dppp, CO, 80 °C; (d) HCl/MeOH (1 M), rt, 2 h; (e) aryl iodide or bromide, CuI, L-proline, NEt_3, DMF, 120 °C; or aryl chloride, DIPEA, DMF, 150 °C; (f) $HONH_2$, NaOH, MeOH, rt; (g) MeI, NaH, DMF, rt; (h) arylsulfonyl chloride, NEt_3, DCM, rt.

Scheme 3. Synthesis of Enantiomers 31 and 32[a]

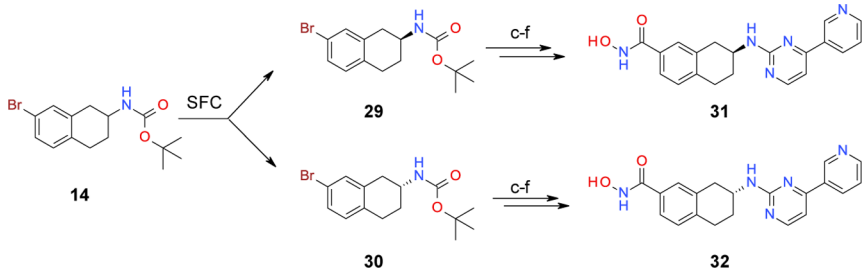

[a]Reagents and conditions: (c) $Pd(OAc)_2$, dppp, CO, 80 °C; (d) HCl/MeOH (1 M), rt, 2 h; (e) aryl iodide or bromide, CuI, L-proline, NEt_3, DMF, 120 °C; or aryl chloride, DIPEA, DMF, 150 °C; (f) $HONH_2$, NaOH, MeOH, rt.

that both **31** and **32** have preferential inhibitory effects on HDAC6 rather than HDAC1–3.

To confirm their HDAC isoform selectivity profile, we tested **31** and **32** in enzymatic inhibition assays. Indeed, both compounds were highly potent against HDAC6 with over 100-fold selectivity over HDAC1 (Table 2). The *R*-configuration may be more favored by HDAC8, as **32** was 4–5 times more potent than **31** in the HDAC8 inhibition assay. Moreover, **32** was only weakly active or inactive to other HDAC isoforms with IC_{50} values above 30 μM. We then tested antiproliferative effects of **32** in several multiple myeloma and neuroblastoma cell lines. Compound **32** was several times weaker than SAHA in cell growth inhibition assays, with GI_{50} values of 7.7 and 5.4 μM against NCI-H929 (multiple myeloma) and BE(2)-C (neuroblastoma) cells, respectively. Compound **32** also induced significantly less cell death in those cell lines than SAHA.

To generate hypotheses about the structural basis of HDAC isoform selectivity, we performed computational docking of enantiomers **31** and **32** into the substrate binding pockets of HDAC1, HDAC6 and HDAC8 using MacroModel and Glide of Schrödinger (Supporting Information). An HDAC6 homology model was generated from structural alignment of HDAC6b with HDAH (histone deacetylase-like amidohydrolase, 1ZZ1 in PDB)[18] in Molecular Operating Environment (MOE) modules. Among several crystal structures of HDAC8, we used the X-ray structure of CRA-A in complex with HDAC8 (1VKG in PDB) for docking studies, considering that CRA-A and its close analogues are selective toward HDAC8 over HDAC1.[19]

dx.doi.org/10.1021/jm5008962 | J. Med. Chem. 2014, 57, 8026–8034

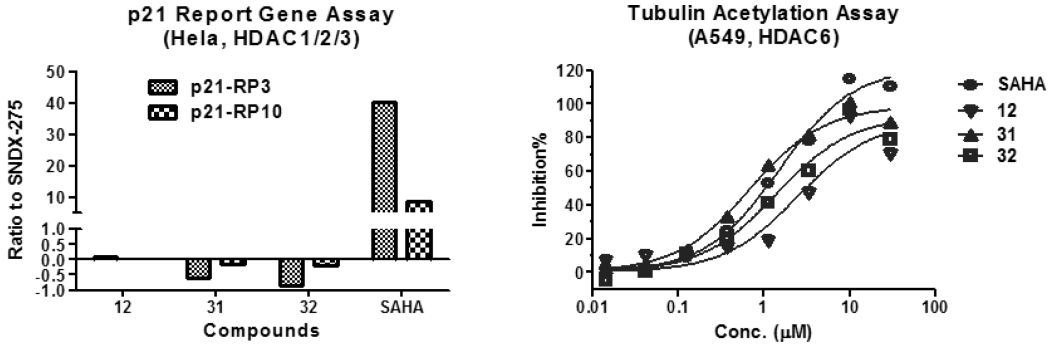

Figure 2. Compounds **31** and **32** do not have impact on p21 induction but induce tubulin acetylation. (A, left) p21 report gene assay in HeLa cells. p21-RP3 represents the relative luciferase signal compared to SNDX-275 at 3 μM. p21-RP10 represents the relative level compared to SNDX-275 at 10 μM. In all cases SD < 10%. (B, right) Tubulin acetylation assay in A549 cells, SD ± 15%.

On the basis of docking predictions, both **31** and **32** should take optimal binding poses and superimpose well with SAHA and **12** in the HDAC6 homology model (Figure 3A). The aminotetralin linker of **31** and **32** is sandwiched between Phe620 and Phe680 in the hydrophobic channel and it forms important hydrophobic interactions similar to the tetrahydroisoquinoline moiety of **12**. These models suggest that the HDAC6 hydrophobic channel could accommodate a bulkier linker than HDAC1 because of the presence of loop 1 in HDAC6 (Supporting Information). In addition, the capping groups are positioned in a wide and shallow pocket in the rim region of HDAC6 and are partially water exposed. This may explain the increased induction of tubulin acetylation by pyrimidine-capped analogues relative to phenyl analogues (e.g., **20** vs **17**) and similar activity against HDAC6 for stereoisomers **31** and **32**.

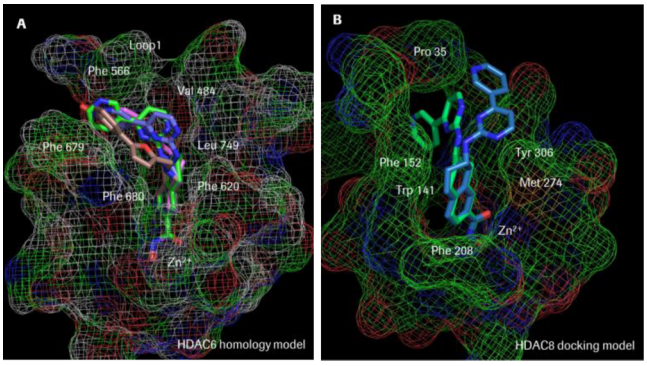

Figure 3. Predicted binding models of **31** and **32** in complex with HDAC6 (A) and HDAC8 (B), respectively. (A) Docking models of SAHA (magenta), **12** (bronze), **31** (blue), and **32** (green) in the HDAC6 homology model to HDAH (1ZZ1 in PDB). (B) Docking models of **31** (blue) and **32** (green) in the CRA-A binding pocket of HDAC8 (1VKG in PDB). For clarity, SAHA and **12** are omitted from (B). HDAC6 and HDAC8 are shown in mesh representation with critical hydrophobic residues labeled in white and carbon atoms in green and gray colors. Oxygen, nitrogen, and sulfur atoms are shown in red, blue, and orange, respectively.

In contrast, it is predicted that **31** and **32** adopt distinct orientations in the rim region of HDAC8 (Figure 3B). The 3-pyridylpyrimidine capping group of **32** fits into a deep and narrow cavity and forms hydrophobic interactions with Pro35, Phe152, and Tyr306 of HDAC8, while the same group of **32** is not in close contact with HDAC8. This is consistent with stronger HDAC8 inhibition by **32** in enzymatic evaluations.

Overall, the 2-*R* configuration of the aminotetralin linker is important to HDAC6 and HDAC8 dual inhibition as **32** showed IC_{50} values of 0.05 and 0.08 μM to them. Furthermore, **32** demonstrated moderate stability in human and mouse liver microsome tests and moderate solubility at 59 μg/mL based on LYSA assay. Accordingly, compound **32** was chosen for further characterization in cellular assays. It has been reported that inhibition of HDAC8 can induce cell differentiation as assessed by morphology and biomarker changes.[14,20] Thus, BE(2)-C cells were treated with **32** at 2 μM for 3 and 9 days and compared with BE(2)-C cells treated with 13-*cis*-retinoic acid (RA) as positive control. As a potent HDAC8 inhibitor, **32** induced neuroblastoma cell differentiation as indicated by the number of neurite outgrowths (Figure 4). Of note, the cell differentiation effect of **32** in BE(2)-C cells appeared to be time dependent. As a comparison, SAHA also induced cell differentiation but was more cytotoxic than **32** under the same conditions.

We then treated BE(2)-C cells with increasing concentrations of SAHA and **32** for 24 h and assessed the resulting changes in several proteins of interest by immunoblot (Figure 5). Both SAHA and **32**, at all tested concentrations, increased levels of acetylated tubulin and TrkA (a cell differentiation marker)[20] compared to vehicle control. In a separate time

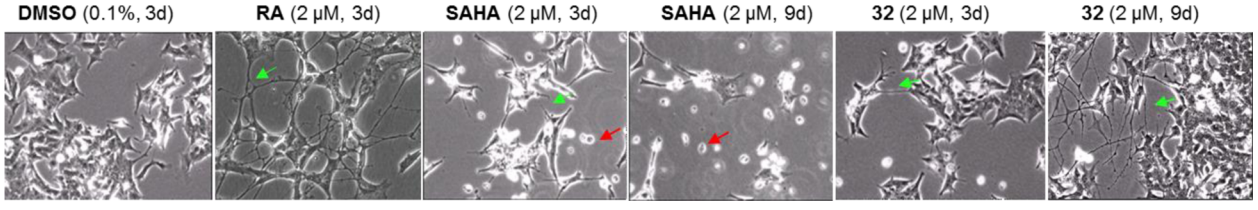

Figure 4. Aminotetralin **32** induces differentiation of neuroblastoma BE(2)-C cells time dependently. Green arrows indicate neurite outgrowth, and red arrows indicate dead cells.

dx.doi.org/10.1021/jm5008962 | J. Med. Chem. 2014, 57, 8026−8034

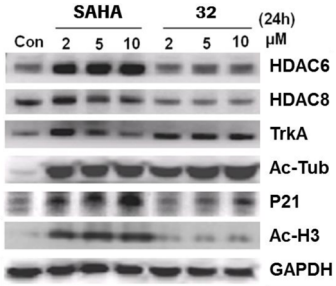

Figure 5. Compound **32** increased Ac-Tub and TrkA but not p21 and Ac-H3 in BE(2)-C cells.

course study, the TrkA expression level correlated with differentiation of BE2C cells (data not shown). Interestingly, SAHA significantly induced HDAC6 but not HDAC8 in BE(2)-C cells. In contrast to SAHA, **32** did not stimulate HDAC6 expression and showed minimal effects on p21 induction and histone H3 acetylation even at 10 μM.

CONCLUSIONS

We have discovered a novel class of HDAC6/8 dual inhibitors with 2-*R*-aminotetralin as a linker and confirmed their HDAC isoform selectivity in biochemical as well as cellular assays. To effectively explore the linker and capping groups, we designed and synthesized a focused library of hydroxamic acids by solid phase synthesis technology. The reductive amination and resin carrier were well suited for the preparation of hydroxamic acids as chemical probe to individual HDAC isoforms. There have been certain debates on the application of enzymatic assays for determination of HDAC selectivity, as the substrates used for individual HDAC isoform profiling may or may not be the relevant substrate for investigating a specific functional role of a given HDAC enzyme that exists as multiprotein complex within the cell.[21] For example, artificial trifluoroacetylated substrates are commonly used to evaluate compound inhibition against purified HDAC4 and HDAC5 enzymes in vitro.[22] Thus, instead of conducting primary screens with standard enzymatic inhibition assays, we used Tub-Ac and p21 induction assays for the identification of putative HDAC6 selective inhibitors and then subsequently confirmed their selectivity profile in enzyme inhibition assays. Our efforts led to the discovery of tetrahydroisoquinoline and aminotetralin moieties as selectivity vectors and linkers for HDAC6/8 dual inhibitors. Treatment of BE(2)-C cells with *R*-aminotetralin **32** resulted in elevated levels of Tub-Ac and induction of TrkA but not p21. Accordingly, compound **32** had weaker antiproliferative effects on cancer cell lines compared with the prototypical pan-HDAC inhibitor SAHA and thus induced differentiation of neuroblastoma cells without significant cytotoxicity. This class of hydroxamates warrants further exploration as selective HDAC6/8 inhibitors for the treatment of multiple myeloma and neuroblastoma based upon the emerging biology of HDAC6 and HDAC8 in these two diseases.

EXPERIMENTAL SECTION

Synthetic Chemistry General Comments. All starting materials were obtained commercially and were used without further purification. All reported yields are of isolated products and are not optimized. Solid phase synthesis was carried out with a MiniBlock from Mettler Toledo. All final compounds were purified by preparative HPLC on reverse phase column using Waters XBridge OBD Phenyl (30 mm × 100 mm, 5 μm) column or OBD RP18 (30 mm × 100 mm, 5 μm) column. For SFC chiral separation, intermediates were separated by chiral column (Daicel chiralpak IC, 5 μm, 30 mm × 250 mm) column using Mettler Teledo SFC-Multigram system: solvent system of 95% CO_2 and 5% IPA (0.5% TEA in IPA), back pressure 100 bar, detection UV 254 nm. Optical rotation was measured in a Rudolph Autopol V automatic polarimeter with wavelength at 589 nm. LC/MS spectra were obtained using a MicroMass Platform LC (Waters Alliance 2795-ZQ2000). NMR spectra were obtained using a Bruker Avance 400 MHz NMR spectrometer. All final compounds have purities greater than 95% based upon LC/MS, and ^{1}H NMR.

*Preparation of Resin **9**.* An amount of 2 g of 4-(hydroxymethyl)-phenoxymethyl-copoly(styrene−1% divinylbenzene) resin ("Wang" resin, 100−200 mesh, 0.75 mmol/g loading, 1.5 mmol) was suspended in dry THF (25 mL) and gently agitated for 30 min. *N*-Hydroxyphthalimide (735 mg, 4.5 mmol) and triphenylphosphane (1.18 g, 4.5 mmol) were added, and the mixture was agitated until these reagents were dissolved. DEAD (783 mg, 4.5 mmol) was added by cannula to give a bright red solution, and the mixture was shaken at rt for 18 h. The resin was washed successively with THF, DMF, DCM, methanol, and finally DCM before being dried in vacuo. The resin was suspended in ethanol/THF (1:3, 20 mL) at 0 °C, and hydrazine hydrate (3 mL) was added. The pale yellow solution was warmed to rt and then gently agitated overnight. Resin **1** was washed with DMF (50 mL), THF (50 mL) under 60 °C and finally with DCM (3 × 20 mL) before dried in vacuo.

*General Procedure for the Preparation of Resin **10**.* Resin **9** (2 g, 0.75 mmol/g loading, 1.5 mmol) was suspended in DMF (40 mL) and gently agitated for 30 min. To this slurry were added *N*-Fmoc protected carboxylic acid (2.25 mmol), HATU (2.28 g, 6 mmol), and DIPEA (774 mg, 6 mmol). The mixture was shaken for 24 h. The resin was collected by filtration, washed successively with DMF (2 × 100 mL), DCM (100 mL), methanol (2 × 100 mL), DCM (100 mL), ether (100 mL), and dried.

*General Procedure for the Preparation of Resin **11**.* Resin 10 (2 g, 0.75 mmol/g loading, 1.5 mmol) was suspended in 20% piperidine/DMF (40 mL) and gently agitated for 30 min. The mixture was shaken for 1 h. The resin was collected by filtration, washed successively with DMF (2 × 100 mL), DCM (100 mL), methanol (2 × 100 mL), DCM (100 mL), ether (100 mL), and dried. Then 200 mg of the obtained resin (0.75 mmol/g loading, 0.15 mmol) was suspended in MeOH/DMF (2:1, 2 mL) and gently agitated for 30 min. To this slurry was added substituted aromatic aldehyde (0.3 mmol) and $NaBH_3CN$ (47 mg, 0.75 mmol). The mixture was shaken for 24 h. The resin was collected by filtration, washed successively with DMF (2 × 100 mL), DCM (100 mL), methanol (2 × 100 mL), DCM (100 mL), ether (100 mL), and dried.

General Procedure for the Resin Cleavage and Preparation of Focused Screening Library. Resin **11** (200 mg, 0.75 mmol/g loading, 0.15 mmol) was suspended in TFA/DCM (1:1, 2 mL) and gently agitated for 30 min. After filtration, the solution was concentrated and the crude product was purified by prep-HPLC.

*2-[[5-(3-Nitrophenyl)-2-furyl]methyl]-3,4-dihydro-1H-isoquinoline-7-carbohydroxamic Acid (**12**).* This compound was prepared by following the SPS procedures as above, with 2-(9*H*-fluoren-9-ylmethoxycarbonyl)-3,4-dihydro-1*H*-isoquinoline-7-carboxylic acid used in the coupling reaction to form resin **2**. HRMS: calcd (MH^+) 394.1397, exp (MH^+) 394.1396. ^{1}H NMR (MeOD, 400 MHz) δ 8.53 (s, 1H), 8.23−8.25 (d, 1H, J = 8.0 Hz), 8.11−8.13 (d, 1H, J = 8.0 Hz), 7.65−7.74 (m, 4H), 7.47−7.48 (d, 1H, J = 4.0 Hz), 7.40−7.42 (d, 1H, J = 8.0 Hz), 4.83 (s, 2H), 4.57 (s, 2 H), 3.68−3.71 (m, 2H), 3.27−3.29 (m, 2H).

*3-(4-Fluoroanilino)tetralin-6-carbohydroxamic Acid (**17**).* A mixture of HCl salt of amine **15** (180 mg, 0.88 mmol), 1-fluoro-4-iodobenzene (124 mg, 0.58 mmol), TEA (0.16 mL, 1.2 mmol), CuI (11 mg, 0.058 mmol), and L-proline (13 mg, 0.116 mmol) in 3 mL of DMF was heated in a microwave reactor at 120 °C for 30 min. After workup with EtOAc and water, the intermediate was mixed with 50% aqueous NH_2OH (1 mL) and KOH (50 mg) in 1 mL of MeOH. After being stirred at rt for 1 h, the mixture was dissolved in EtOAc, washed

dx.doi.org/10.1021/jm5008962 | J. Med. Chem. 2014, 57, 8026−8034

with water, and concentrated. The crude product was purified by HPLC. MS: calcd (MH^+) 301.1, exp (MH^+) 301.1. HRMS: calcd (MH^+) 301.1347, exp (MH^+) 301.1346. ^{1}HNMR (CD_3OD, 400 MHz) δ 7.52 (d, 2H, J = 8.0 Hz), 7.24 (m, 1H), 7.12 (m, 4H), 3.85 (m, 1H), 3.22 (m, 1H), 3.05−2.84 (m, 3H), 2.26 (m, 1H), 1.78 (m, 1H).

*3-(3-Chloro-4-cyanoanilino)tetralin-6-carbohydroxamic Acid (**18**).* MS: calcd (MH^+) 342.1, exp (MH^+) 342.1. HRMS: calcd (MH^+) 342.1004, exp (MH^+) 342.1004. ^{1}H NMR (CD_3OD, 400 MHz) δ 7.64 (m, 2H), 7.51 (m, 2H), 7.24 (d, 1H, J = 8.8 Hz), 6.95 (d, 1H, J = 8.8 Hz), 3.98 (m, 1H), 3.27 (m, 1H), 3.04 (m, 2H), 2.97 (m, 1H), 2.24 (m, 1H), 1.87 (m, 1H).

*3-(2-Pyridylamino)tetralin-6-carbohydroxamic Acid (**19**).* MS: calcd (MH^+) 284.1, exp (MH^+) 284.3. HRMS: calcd (MH^+) 284.1394, exp (MH^+) 284.1395. ^{1}H NMR (CD_3OD, 400 MHz) δ 7.85−7.93 (m,2H), 7.55 (m, 2H), 7.25 (d, 1H, J = 8 Hz), 7.12 (d, 1H, J = 8.8 Hz), 6.92 (t, 1H, J = 6.4 Hz), 4.79 (m, 1H), 2.8−3.2 (m, 4H), 2.2 (m, 1H), 1.9 (m, 1H).

*3-(Pyrimidin-2-ylamino)tetralin-6-carbohydroxamic Acid (**20**).* A mixture of **15** (60 mg), 2-chloropyrimidine (50 mg), and TEA (0.2 mL) in 2 mL of DMF was heated at 150 °C for 1 h in a microwave reactor. After concentration, the crude product was dissolved in 1 mL of MeOH and mixed with a solution of 50% aqueous NH_2OH (1 mL) and KOH (50 mg). After being stirred at rt for 1 h, the mixture was concentrated and purified by HPLC. MS: calcd (MH^+) 285.1, exp (MH^+) 285.3. HRMS: calcd (MH^+) 285.1346, exp (MH^+) 285.1346. ^{1}H NMR (CD_3OD, 400 MHz) δ 8.42 (d, 2H, J = 4.8 Hz), 7.22−7.52 (m, 3H), 6.8 (d, 1H, J = 4.8 Hz), 4.30 (m, 1H), 2.8−3.2 (m, 4H), 2.25 (m, 1H), 1.9 (m, 1H).

*3-[(4-Phenylpyrimidin-2-yl)amino]tetralin-6-carbohydroxamic Acid (**21**).* MS: calcd (MH^+) 361.1, exp (MH^+) 361.4. HRMS: calcd (MH^+) 361.1659, exp (MH^+) 361.1658. ^{1}H NMR (CD_3OD, 400 MHz) δ 8.34 (d, 1H, J = 6 Hz), 8.22 (d, 2H, J = 7.6 Hz), 7.5−7.7 (m, 5H), 7.42 (d, 1H, J = 5.6 Hz), 7.25 (d, 1H, J=8 Hz), 4.41 (s, 1H), 3.30 (m, 1H), 2.9−3.07 (m, 3H), 2.29 (m, 1H), 1.98 (m, 1H).

*3-[[4-(4-Chlorophenyl)pyrimidin-2-yl]amino]tetralin-6-carbohydroxamic Acid (**22**).* MS: calcd (MH^+) 395.1, exp (MH^+) 395.2. HRMS: calcd (MH^+) 395.1269, exp (MH^+) 395.1268. ^{1}H NMR (CD_3OD, 400 MHz) δ 8.35 (d, 1H, J = 6.0 Hz), 8.20 (d, 2H, J = 8.4 Hz), 7.55 (m, 4H), 7.35 (d, 1H, J = 5.6 Hz), 7.25 (d, 1H, J = 8.0 Hz), 4.41 (s, 1H), 3.30 (m, 1H), 3.05 (t, 2H, J = 5.6 Hz), 2.90 (m, 1H), 2.28 (m, 1H), 1.94 (m, 1H).

*3-[[4-(3-Chlorophenyl)pyrimidin-2-yl]amino]tetralin-6-carbohydroxamic Acid (**23**).* MS: calcd (MH^+) 395.1, exp (MH^+) 395.2. HRMS: calcd (MH^+) 395.1269, exp (MH^+) 395.1267. ^{1}H NMR (CD_3OD, 400 MHz) δ 8.35 (d, 1H, J = 5.2 Hz), 8.14 (m, 1H), 8.02 (m, 1H), 7.46−7.54 (m, 4H), 7.25 (d, 1H, J = 8.4 Hz), 7.15 (d, 1H, J = 5.2 Hz), 4.41 (s, 1H), 3.30 (m, 1H), 3.05 (t, 2H, J = 5.6 Hz), 2.90 (m, 1H), 2.28 (m, 1H), 1.94 (m, 1H).

*3-[[4-(2-Chlorophenyl)pyrimidin-2-yl]amino]tetralin-6-carbohydroxamic Acid (**24**).* MS: calcd (MH^+) 395.1, exp (MH^+) 395.2. ^{1}H NMR (CD_3OD, 400 MHz) δ 8.35 (d, 1H, J = 4.8 Hz), 7.60 (m, 1H), 7.54 (m, 3H), 7.43 (m, 2H), 7.22 (d, 1H, J = 8.4 Hz), 6.90 (d, 1H, J = 5.2 Hz), 4.41 (s, 1H), 3.30 (m, 1H), 3.05 (t, 2H, J = 5.6 Hz), 2.90 (m, 1H), 2.28 (m, 1H), 1.94 (m, 1H).

*3-[[4-(3-Pyridyl)pyrimidin-2-yl]amino]tetralin-6-carbohydroxamic Acid (**25**).* MS: calcd (MH^+) 362.1, exp (MH^+) 362.4. HRMS: calcd (MH^+) 362.1612, exp (MH^+) 362.1610. ^{1}H NMR (CD_3OD, 400 MHz) δ 9.48 (s, 1H), 8.99 (d, 1H, J = 8 Hz), 8.88 (s, 1H), 8.48 (d, 1H, J = 4.8 Hz), 7.99 (m, 1H), 7.52 (m, 2H), 7.43 (d, 1H, J = 4.4 Hz), 7.24 (d, 1H, J = 8.4 Hz), 2.8−3.2 (m, 5H), 2.29 (m, 1H), 2.00 (m, 1H).

*3-[Methyl-[4-(3-pyridyl)pyrimidin-2-yl]amino]tetralin-6-carbohydroxamic Acid (**26**).* MS: calcd (MH^+) 376.1, exp (MH^+) 376.4. HRMS: calcd (MH^+) 376.1768, exp (MH^+) 376.1766. ^{1}H NMR (CD_3OD, 400 MHz) δ 9.34 (s, 1H), 8.72 (m, 2H), 8.50 (d, 1H, J = 4.8 Hz), 7.5 (m, 1H), 7.4−7.5 (m, 4 Hz), 5.20 (s, 2H), 3.2 (s, 3H), 2.9−3.07 (m, 4H), 2.12 (m, 2H).

*3-[(3-Fluorophenyl)sulfonylamino]tetralin-6-carbohydroxamic Acid (**27**).* A mixture of HCl salt of amine **11**, 3-fluorobenzenesulfonyl chloride, and TEA in DCM was stirred for 30 min and concentrated. The ester intermediate was treated with aqueous NH_2OH (1 mL) and KOH (50 mg), and the crude product was purified by HPLC. MS: calcd (MH^+) 365.1, exp (MH^+) 365.4. HRMS: calcd (MH^+) 365.0966, exp (MH^+) 365.0965. ^{1}H NMR (CD_3OD, 400 MHz), 7.75 (d, 1H, J = 8.0 Hz) δ 7.60−7.66 (m, 2H), 7.46 (d, 1H, J = 8.0 Hz), 7.41 (m, 1H), 7.36 (s, 1H), 7.14 (d, 1H, J = 8.0 Hz), 3.55 (m, 1H), 2.95 (m, 2H), 2.82 (m, 1H), 2.69 (m, 1H), 1.95 (m, 1H) 1.73 (m, 1H).

*3-[(3-Chlorophenyl)sulfonylamino]tetralin-6-carbohydroxamic Acid (**28**).* MS: calcd (MH^+) 381.1, exp (MH^+) 381.2. HRMS: calcd (MH^+) 381.0670, exp (MH^+) 381.0668. ^{1}H NMR (CD_3OD, 400 MHz), 7.90 (m, 1H), 7.84 (d, 1H, J = 8.0 Hz) δ 7.66 (d, 1H, J = 8.4 Hz), 7.59 (t, 1H, J = 8.0 Hz), 7.47 (d, 1H, J = 8.0 Hz), 7.36 (s, 1H), 7.15 (d, 1H, J = 8.0 Hz), 3.55 (m, 1H), 2.95 (m, 2H), 2.82 (m, 1H), 2.69 (m, 1H), 1.95 (m, 1H) 1.73 (m, 1H).

*(3S)-3-[[4-(3-Pyridyl)pyrimidin-2-yl]amino]tetralin-6-carbohydroxamic Acid (**31**).* Compound **31** was prepared from chiral intermediate **29** after SFC separation of **14**. MS: calcd (MH^+) 362.1, exp (MH^+) 362.1. ^{1}H NMR (CD_3OD, 400 MHz) δ 9.55 (s, 1H), 9.13 (d, 1H, J = 6.8 Hz), 8.95 (s, 1H), 8.52 (d, 1H, J = 4.8 Hz), 8.07 (m, 1H), 7.53 (m, 3H), 7.24(m, 1H), 3.34(m,1H), 2.9−3.07 (m, 4H), 2.29 (m, 1H), 1.98 (m, 1H).

*(3R)-3-[[4-(3-Pyridyl)pyrimidin-2-yl]amino]tetralin-6-carbohydroxamic Acid (**32**).* Compound **32** was prepared from chiral intermediate **29** after SFC separation of **14**. Optical rotation, $[\alpha]_D^{20}$ +45.2° (0.115% g/100 mL, MeOH). MS: calcd (MH^+) 362.1, exp (MH^+) 362.2. HRMS: calcd (MH^+) 362.1612, exp (MH^+) 362.1610. ^{1}H NMR (CD_3OD, 400 MHz) δ 9.51 (s, 1H), 9.08 (d, 1H, J = 7.6 Hz), 8.92 (m, 1H), 8.51 (d, 1H, J = 4.8 Hz), 8.00 (m, 1H), 7.52 (m, 3H), 7.25 (d, 1H, 7.6 Hz), 3.34 (m,1H), 2.9−3.07 (m, 4H), 2.29 (m, 1H), 1.98 (m, 1H).

Molecular Modeling. Homology modeling and molecular dynamics simulations were conducted in the molecular operating environment (MOE), and geometric optimizations of compounds and molecular docking were finished by MacroModel and Glide of Schrödinger, respectively. The sequence corresponding to HDAC6b was aligned with that of HDAH in the MOE-Align module. The HDAC6 homology model was constructed by using 1ZZ1 (PDB) as template, and the final model was taken as the Cartesian average of all the intermediate models and was further refined by molecular dynamic simulations and energy minimizations, during which only the side chains of all residues were allowed to move. The molecular dynamics simulations were set to 5 ps of heating to 300 K, 10 ps of equilibrium at 300 K, and 5 ps of cooling to 0 K. For docking studies in HDAC8, the cocrystal structure of CRA-A in complex with HDAC8 (1VKG in PDB) was used. OPLS_2005 force field of MacroModel was used to optimize the initial geometries of the compounds with a final root-mean-square gradient of 0.01 kcal mol^{-1} $Å^{-1}$. The default values of the optimization parameters and thresholds were kept. All torsion angles of compound were released to freely rotate, and 10 000 docking runs were adopted during the XP docking with NE2 atom of His residues and zinc ion as docking constraints. Docking poses were clustered based on heavy atom rmsd values (0.5 Å), and top-ranked poses of each compound were selected and viewed graphically within Maestro of the Schrödinger program and finally displayed in Pymol.

Microsomal Stability Assay. Each incubated mixture contained 0.5 mg/mL liver microsome (human or mouse), 100 mM potassium phosphate buffer (pH 7.4), 10 mM NADPH, and 1 μM test compound in a total volume of 400 μL. After prewarming at 37 °C for 10 min, the NADPH was added to initiate the reaction. Reaction was terminated after 0, 3, 6, 9, 15, and 30 min by adding 150 μL of 100 ng/mL of tolbutamide (internal standard) in ice cold methanol into 300 μL of incubation mixtures. Samples were then centrifuged at 4000 rpm for 10 min at 4 °C. The supernatant was then analyzed by LC−MS/MS.

LYSA Solubility Assay. An amount of 150 μL of 10 mM DMSO stock solution of compound was prepared and divided into two portions. For one portion the DMSO solution was evaporated to dryness at 35 °C in a centrifugal vacuum evaporator from Genevac Technologies, and the remaining was redissolved in 50 mM phosphate buffer (pH 6.5). The mixture was stirred and shaken for 1−2 h. After

an overnight stand, the solution was filtered before HPLC analysis. The other portion was used for the calibration curve preparation by diluting the DMSO stock solution using the same PBS buffer mentioned above to a series of solutions with concentration range of 50−500 μM.

Biology General Comments. Brief descriptions of the biological protocols used to generate data in this manuscript can be found below. All growth media included 100 units/mL penicillin and 100 μg/mL streptomycin, and all cell lines were grown in 5% CO_2 at 37 °C. NCI-H929, A549, HeLa, OPM-2, and BE(2)-C cells were obtained from ATCC. Mammalian protein extraction reagent and tissue protein extraction reagent were obtained from Thermo Scientific. EDTA-free protease inhibitors were obtained from Roche Diagnostics. Monoclonal anti-p21 antibody and antiacetylated histone H3 (Ac 1−20) antibodies were purchased from Calbiochem. Anti-TrkA and anti-HDAC6 were from Cell Signaling Technology. Anti-HDAC8 was from Millipore. HRP-conjugated monoclonal anti-GAPDH, peroxidase-conjugated goat anti-rabbit IgG and anti-mouse IgG were purchased from KangChen. Enhanced chemiluminescence (ECL) detection kit was obtained from Thermo Scientific.

Tubulin Acetylation (Tub-Ac) Cytoblot Assay. Tubulin acetylation was detected by the antiacetylated tubulin antibody (Sigma) and horseradish peroxidase (HRP) conjugated secondary antibody (KangChen Bio-Tech). A549 cells were seeded into assay plates (Corning 3912) at a concentration of 1×10^5 cells/mL and incubated for 16−18 h at 37 °C in the presence of 5% CO_2. Then 20 μL of diluted compound solution was transferred to the cell culture plate and incubated for 17−18 h. After medium removal and fixation by formaldehyde (3.7% paraformaldehyde in TBS), the cells in the plates were treated with 180 μL of −20 °C MeOH and incubated for 5 min at rt. The cell lysis was incubated with 75 μL of primary antiacetylated tubulin antibody and secondary HRP conjugated antibody solution (1:750 antiacetylated tubulin, 1:750 HRP conjugated anti-mouse IgG in antibody dilution buffer not containing sodium azide) for 4 h at 4 °C. Then 75 μL of enhanced chemiluminescence (ECL) reagent was added into the wells, and the luminescence from each well was immediately quantified by the plate reader. On the basis of the luminescence reading, the EC_{50} values against Tub-Ac were calculated by plotting the curve with XLfit 4.0 software.

p21 Reporter Gene Assay. Compounds were tested for their ability to induce p21 gene expression using a reporter gene assay involving HeLa cells transfected with a p21 promoter−luciferase construct. The p21 promoter has the Sp1/Sp3 binding site for HDAC but not the upstream p53 binding site. Briefly, the day before transfection, HeLa cells were seeded at 11 000 cells/well in a 96-well culture plate and incubated at 37 °C in 5% CO_2 overnight. For transfection, the medium was removed and replaced with 100 μL/well transfection media prepared by following procedure: 5 μL of serum-free DMEM, 0.15 μL of Fugene 6 reagent, 40 ng of p21-luc, and 10 ng of GFP were mixed and incubated at room temperature for 30 min. Then 98 μL of DMEM (with 10% FBS, 1% penicillin and streptomycin) was added to the DNA/Fugene 6 reagent complex and mixed gently. After incubation of the cells for 24 h at 37 °C under 5% CO_2, fresh medium and test compounds were added to the wells and incubated for 15 h. Cells were lysed by adding 80 μL/well of culture lysis reagent (Promega). An amount of 50 μL of each lysate was taken for GFP detection using an excitation wavelength of 486 nm and detection at 527 nm. Then 100 μL of luciferase assay reagent (Promega) was added to 20 μL of cell lysate for luminometer reading. The relative gene level of p21 induced by individual compound was compared to SNDX-275 at 1, 3, and 10 μM concentrations.

HDAC Enzyme Inhibition Assay. HDAC enzyme inhibition assays were conducted by Reaction Biology Corporation using a 10-point dose−response curve with half-log serial dilutions, fluorogenic peptides at 50 μM as enzymatic substrate, and trichostatin A as a positive control unless otherwise indicated. TMP-269 was used as positive control for the testing of **31** and **32** against class IIa HDACs (HDAC4, HDAC5, HDAC7, and HDAC9). See details at www.reactionbiology.com.

Cell Proliferation (Water-Soluble Tetrazolium Dye) Assay. Cells were seeded in 96-well culture plates (200 μL/well at different seeding concentrations depending on cell type) and incubated overnight at 37 °C in 5% CO_2. After addition of compound (typically eight-point half-log serial dilutions in triplicate) to the cells (DMSO concentration kept below 0.5%), the cell culture was incubated at 37 °C in 5% CO_2 for 72 h. The effects on proliferation were determined by addition of CCK-8 reagent (Dojindo) according to the manufacturer's instruction, followed by a 2 h incubation at 37 °C in 5% CO_2 and detection of the absorbance at 450 nm using an ELISA plate reader.

Western Blotting. 1×10^6 BE(2)-C cells were seeded overnight and then incubated with indicated concentrations of SAHA and **32** for 24 h. Cell extract was prepared by lysing cultured cells with a mammalian protein extraction reagent supplemented with EDTA-free protease inhibitor for 15 min. Supernatants were collected following centrifugation of lysed cells (15 000 g) for 10 min at 4 °C. To analyze the cell lysate, 30 μg of total protein per sample was resolved by SDS−PAGE and transferred onto nitrocellulose membrane. Membranes with immobilized proteins were probed with antibodies for HDAC6, HDAC8, TrkA, Tub-Ac, and p21. The reactive protein bands were visualized using an enhanced chemiluminescence (ECL) detection system.

■ ASSOCIATED CONTENT

Ⓢ Supporting Information

Detailed experimental procedures for the synthesis of solid phase library, and additional biological profiling of **12**, **31**, and **32**. This material is available free of charge via the Internet at http://pubs.acs.org.

■ AUTHOR INFORMATION

Corresponding Author

*Phone: +86 21 38954910, extension 3350. Fax: +86 21 50790291. E-mail: gordon.tang@roche.com.

Present Address

†J.C.W.: 14 Moonbeam Drive, Mountain View, CA 94043, U.S.

Notes

The authors declare no competing financial interest.

■ ACKNOWLEDGMENTS

We are grateful to Sheng Zhong, Wenzhi Cheng, Qinshan Gao, and Peilan Ding for their analytical assistance and purification of final compounds. We also thank Yuxia Zhang, Yi Zhang, Hongxia Qiu, and Xiaoyue Wu for carrying out the physicochemical and microsome stability studies.

■ ABBREVIATIONS USED

HDAC, histone deacetylase; RA, 13-*cis*-retinoic acid; SAHA, suberoylanilide hydroxamic acid; SAR, structure−activity relationship; ZBG, zinc-binding group

■ REFERENCES

(1) Minucci, S.; Pelicci, P. G. Histone deacetylase inhibitors and the promise of epigenetic (and more) treatments for cancer. *Nat. Rev. Cancer* **2006**, *6*, 38−51.

(2) (a) Weiwer, M.; Lewis, M. C.; Wagner, F. F.; Holson, E. B. Therapeutic potential of isoform selective HDAC inhibitors for the treatment of schizophrenia. *Future Med. Chem.* **2013**, *5*, 1491−1508. (b) McKinsey, T. A. Isoform-selective HDAC inhibitors: closing in on translational medicine for the heart. *J. Mol. Cell. Cardiol.* **2011**, *51*, 491−496.

(3) Wong, J. C.; Hong, R.; Schreiber, S. L. Structural biasing elements for in-cell histone deacetylase paralog selectivity. *J. Am. Chem. Soc.* **2003**, *125*, 5586−5587.

(4) Santo, L.; Hideshima, T.; Kung, A. L.; Tseng, J. C.; Tamang, D.; Yang, M.; Jarpe, M.; van Duzer, J. H.; Mazitschek, R.; Ogier, W. C.; Cirstea, D.; Rodig, S.; Eda, H.; Scullen, T.; Canavese, M.; Bradner, J.; Anderson, K. C.; Jones, S. S.; Raje, N. Preclinical activity, pharmacodynamic, and pharmacokinetic properties of a selective HDAC6 inhibitor, ACY-1215, in combination with bortezomib in multiple myeloma. *Blood* **2012**, *119*, 2579−2589.
(5) (a) Butler, K. V.; Kalin, J.; Brochier, C.; Vistoli, G.; Langley, B.; Kozikowski, A. P. Rational design and simple chemistry yield a superior, neuroprotective HDAC6 inhibitor, tubastatin A. *J. Am. Chem. Soc.* **2010**, *132*, 10842−10846. (b) Kalin, J. H.; Butler, K. V.; Akimova, T.; Hancock, W. W.; Kozikowski, A. P. Second-generation histone deacetylase 6 inhibitors enhance the immunosuppressive effects of Foxp3+ T-regulatory cells. *J. Med. Chem.* **2012**, *55*, 639−651.
(6) Lee, J. H.; Mahendran, A.; Yao, Y. S.; Ngo, L.; Venta-Perez, G.; Choy, M. L.; Kim, N.; Ham, W. S.; Breslow, R.; Marks, P. A. Development of a histone deacetylase 6 inhibitor and its biological effects. *Proc. Natl. Acad. Sci. U.S.A.* **2013**, *110*, 15704−15709.
(7) Wagner, F. F.; Olson, D. E.; Gale, J. P.; Kaya, T.; Weiwer, M.; Aidoud, N.; Thomas, M.; Davoine, E. L.; Lemercier, B. C.; Zhang, Y. L.; Holson, E. B. Potent and selective inhibition of histone deacetylase 6 (HDAC6) does not require a surface-binding motif. *J. Med. Chem.* **2013**, *56*, 1772−1776.
(8) Balasubramanian, S.; Ramos, J.; Luo, W.; Sirisawad, M.; Verner, E.; Buggy, J. J. A novel histone deacetylase 8 (HDAC8)-specific inhibitor PCI-34051 induces apoptosis in T-cell lymphomas. *Leukemia* **2008**, *22*, 1026−1034.
(9) (a) Suzuki, T.; Ota, Y.; Ri, M.; Bando, M.; Gotoh, A.; Itoh, Y.; Tsumoto, H.; Tatum, P. R.; Mizukami, T.; Nakagawa, H.; Iida, S.; Ueda, R.; Shirahige, K.; Miyata, N. Rapid discovery of highly potent and selective inhibitors of histone deacetylase 8 using click chemistry to generate candidate libraries. *J. Med. Chem.* **2012**, *55*, 9562−9575. (b) Suzuki, T.; Muto, N.; Bando, M.; Itoh, Y.; Masaki, A.; Ri, M.; Ota, Y.; Nakagawa, H.; Iida, S.; Shirahige, K.; Miyata, N. Design, synthesis, and biological activity of NCC149 derivatives as histone deacetylase 8-selective inhibitors. *ChemMedChem* **2014**, *9*, 657−664.
(10) Khan, N.; Jeffers, M.; Kumar, S.; Hackett, C.; Boldog, F.; Khramtsov, N.; Qian, X. Z.; Mills, E.; Berghs, S. C.; Carey, N.; Finn, P. W.; Collins, L. S.; Tumber, A.; Ritchie, J. W.; Jensen, P. B.; Lichenstein, H. S.; Sehested, M. Determination of the class and isoform selectivity of small-molecule histone deacetylase inhibitors. *Biochem. J.* **2008**, *409*, 581−589.
(11) Liu, L.; Chen, B.; Qin, S.; Li, S.; He, X.; Qiu, S.; Zhao, W.; Zhao, H. A novel histone deacetylase inhibitor chidamide induces apoptosis of human colon cancer cells. *Biochem. Biophys. Res. Commun.* **2010**, *392*, 190−195.
(12) Wong, J. C.; Tang, G.; Wu, X.; Liang, C.; Zhang, Z.; Guo, L.; Peng, Z.; Zhang, W.; Lin, X.; Wang, Z.; Mei, J.; Chen, J.; Pan, S.; Zhang, N.; Liu, Y.; Zhou, M.; Feng, L.; Zhao, W.; Li, S.; Zhang, C.; Zhang, M.; Rong, Y.; Jin, T. G.; Zhang, X.; Ren, S.; Ji, Y.; Zhao, R.; She, J.; Ren, Y.; Xu, C.; Chen, D.; Cai, J.; Shan, S.; Pan, D.; Ning, Z.; Lu, X.; Chen, T.; He, Y.; Chen, L. Pharmacokinetic optimization of class-selective histone deacetylase inhibitors and identification of associated candidate predictive biomarkers of hepatocellular carcinoma tumor response. *J. Med. Chem.* **2012**, *55*, 8903−8925.
(13) (a) Yang, P. H.; Zhang, L.; Zhang, Y. J.; Zhang, J.; Xu, W. F. HDAC6: physiological function and its selective inhibitors for cancer treatment. *Drug Discoveries Ther.* **2013**, *7*, 233−242. (b) Zhang, L.; Sheng, S.; Qin, C. The role of HDAC6 in Alzheimer's disease. *J. Alzheimer's Dis.* **2013**, *33*, 283−295. (c) Valenzuela-Fernandez, A.; Cabrero, J. R.; Serrador, J. M.; Sanchez-Madrid, F. HDAC6: a key regulator of cytoskeleton, cell migration and cell-cell interactions. *Trends Cell Biol.* **2008**, *18*, 291−297. (d) Dallavalle, S.; Pisano, C.; Zunino, F. Development and therapeutic impact of HDAC6-selective inhibitors. *Biochem. Pharmacol.* **2012**, *84*, 756−765.
(14) Oehme, I.; Deubzer, H. E.; Lodrini, M.; Milde, T.; Witt, O. Targeting of HDAC8 and investigational inhibitors in neuroblastoma. *Expert Opin. Invest. Drugs* **2009**, *18*, 1605−1617.
(15) Olson, D. E.; Wagner, F. F.; Kaya, T.; Gale, J. P.; Aidoud, N.; Davoine, E. L.; Lazzaro, F.; Weïwer, M.; Zhang, Y.-L.; Holson, E. B. Discovery of the first histone deacetylase 6/8 dual inhibitors. *J. Med. Chem.* **2013**, *56*, 4816−4820.
(16) Hubbert, C.; Guardiola, A.; Shao, R.; Kawaguchi, Y.; Ito, A.; Nixon, A.; Yoshida, M.; Wang, X. F.; Yao, T. P. HDAC6 is a microtubule-associated deacetylase. *Nature* **2002**, *417*, 455−458.
(17) Wong, J. C.; Guo, L.; Peng, Z.; Zhang, W.; Zhang, N.; Lai, W.; Zhang, Z.; Zhang, C.; Zhang, X.; Song, S.; Pan, D.; Xie, C.; Li, J.; Ning, Z.; Lu, X.; He, Y.; Chen, L. Application of p21 and klf2 reporter gene assays to identify selective histone deacetylase inhibitors for cancer therapy. *Bioorg. Med. Chem. Lett.* **2011**, *21*, 110−116.
(18) Nielsen, T. K.; Hildmann, C.; Dickmanns, A.; Schwienhorst, A.; Ficner, R. Crystal structure of a bacterial class 2 histone deacetylase homologue. *J. Mol. Biol.* **2005**, *354*, 107−120.
(19) Vannini, A.; Volpari, C.; Filocamo, G.; Casavola, E. C.; Brunetti, M.; Renzoni, D.; Chakravarty, P.; Paolini, C.; De Francesco, R.; Gallinari, P.; Steinkuhler, C.; Di Marco, S. Crystal structure of a eukaryotic zinc-dependent histone deacetylase, human HDAC8, complexed with a hydroxamic acid inhibitor. *Proc. Natl. Acad. Sci. U.S.A.* **2004**, *101*, 15064−15069.
(20) Shikata, A.; Shikata, T.; Sotozono, Y.; Hosoi, H.; Matsumura, T.; Sugimoto, T.; Sawada, T. Neuronal differentiation in human neuroblastoma cells by nerve growth factor following TrkA up-regulation by interferon-gamma. *Med. Pediatr. Oncol.* **2000**, *34*, 394−401.
(21) Bantscheff, M.; Hopf, C.; Savitski, M. M.; Dittmann, A.; Grandi, P.; Michon, A. M.; Schlegl, J.; Abraham, Y.; Becher, I.; Bergamini, G.; Boesche, M.; Delling, M.; Dumpelfeld, B.; Eberhard, D.; Huthmacher, C.; Mathieson, T.; Poeckel, D.; Reader, V.; Strunk, K.; Sweetman, G.; Kruse, U.; Neubauer, G.; Ramsden, N. G.; Drewes, G. Chemoproteomics profiling of HDAC inhibitors reveals selective targeting of HDAC complexes. *Nat. Biotechnol.* **2011**, *29*, 255−265.
(22) Lahm, A.; Paolini, C.; Pallaoro, M.; Nardi, M. C.; Jones, P.; Neddermann, P.; Sambucini, S.; Bottomley, M. J.; Lo Surdo, P.; Carfi, A.; Koch, U.; De Francesco, R.; Steinkuhler, C.; Gallinari, P. Unraveling the hidden catalytic activity of vertebrate class IIa histone deacetylases. *Proc. Natl. Acad. Sci. U.S.A.* **2007**, *104*, 17335−17340.